Submitted to the International Journal of Robotics Research, Sage Publications Ltd.

# Biomimetic Centering Behavior for Undulatory Robots*

Michael Sfakiotakis and Dimitris P. Tsakiris†

*Computational Vision and Robotics Laboratory*
*Institute of Computer Science - FORTH*
*Vassilika Vouton, P.O. Box 1385, GR-71110 Heraklion, Greece*
{*sfakios, tsakiris*}*@ics.forth.gr*

**Abstract**

Substantial work exists in the robotics literature on the mechanical design, modeling, gait generation and implementation of undulatory robotic prototypes. However, there appears to have been relatively limited work on closing the control loop, for such robotic locomotors, using sensory information from exteroceptive sensors, thus leading to more complex reactive undulatory behaviors.

This paper considers a biologically-inspired sensor-based centering behavior for undulatory robots; such behaviors have been observed and studied in bees, and robotic analogs were originally developed for nonholonomic mobile robots. Adaptation to the significantly more complex dynamics of undulatory locomotors highlights a number of issues related to the use of sensors (possibly distributed over the elongated body of the mechanism) for the generation of reactive undulatory behaviors, to biomimetic neuromuscular control and to formation control of multi-undulatory swarms. These issues are explored in simulation via computational tools specifically geared towards undulatory locomotion in robotics and biology. A series of undulatory robotic prototypes has been developed, which are able to propel themselves on hard floor, on foam elastic material, on sand, etc., both in eel-like and in polychaete-like undulatory modes. These prototypes have been equipped with infrared distance sensors, and are used to demonstrate experimentally the undulatory centering behavior in several corridor-like environments.

KEY WORDS - biomimetic robotics, undulatory locomotion, reactive behaviors, exteroceptive sensors

## 1 Introduction

Undulatory robotic locomotors are serially connected, multilink articulated mechanisms, which propel themselves by body shape undulations. Advantages associated with them include terrain adaptability, modularity and redundancy, as well as their potential for use as combined locomotors and manipulators [1–3]. Biological organisms provide inspiration for the design and development of such mechanisms, as locomotion by transversal whole-body waves is widespread among elongated narrow animals (snakes, eels, marine worms, nematodes, larvae, etc.). While most of the existing such robots utilize passive wheels to realize serpentine locomotion (see [1–6] and references therein), more recent work addresses undulatory prototypes which crawl on their underside, and do not rely on wheels (e.g., [7–12]), as well as undulatory swimming robots (e.g., [2, 13–16]). The great majority of these prototypes, both aquatic and terrestrial, employ

*This work was supported in part by the European Commission, through the IST projects BIOLOCH (IST-2001-34181) and MATHESIS (FP6-027574).

†Corresponding author.

head-to-tail transversal waves for forward propulsion (designated here as *eel-like* undulatory locomotion). Recent investigations of robotic prototypes which utilize a tail-to-head body wave for forward propulsion (designated here as *polychaete-like* undulatory locomotion) are presented in [11,12,17].

The undulatory robotics literature has mainly focused on mechanical design and open-loop control (gait generation). Trajectory tracking for, mainly wheeled, snake-like robots, has been studied, either assuming that perfect system state information is available, or using position information from an external vision system (e.g., [6,6,8,15,18,19]). However, on-board exteroceptive sensors appear to be necessary in order to enhance the autonomy of the undulatory robots, so that they become able to operate in the complex environments for which they are intended. In this case, closed-loop control schemes for navigating these robots, via the modulation of the joint oscillation parameters, are needed. Some first steps in this direction consider either, at a lower level, sensing modalities (e.g., pressure) used to identify substrate properties and select an appropriate gait over varying terrain [20], or, at a higher level, exteroceptive sensors (e.g., distance, vision) allowing the implementation of more complex behaviors (e.g., obstacle avoidance, pursuit of moving targets, formation control). One of the first such investigations appears to be the ACM-III wheeled serpentine robot, which is equipped with tactile sensors along its body, and demonstrates advancement inside narrow labyrinths and adaptive coiling around objects [1,2]. The GMD snake robots feature tactile sensors, infrared sensors, cameras and lasers for applications like pipeline inspection [7,21,22]. The lamprey robot of [13] uses a compass, inclinometers and sonars to enable behavior switches in response to environmental perturbations. The undulatory mechanism of [23] features a camera mounted on its head link, which is used to track a trajectory specified by a black strip on the ground. Finally, in [24], on-board distance sensors are used to determine orientation errors in the direction of locomotion.

Many potential applications of undulatory robots (e.g., site inspection, search-and rescue missions, mine clearance) involve tasks which could be efficiently addressed by multiple robotic agents operating in a cooperative manner. A significant body of work is available regarding the dynamics and control of swarms, but either for conventional mobile robots, or for underwater and aerial vehicles [25–30], while sensor-based aspects of these control problems are addressed in, e.g., [27–29]. However, despite their potential importance, swarms of undulatory robots do not appear to have been investigated.

This paper considers a biologically-inspired sensor-based centering behavior for undulatory robots, whose dynamics and gait generation are briefly addressed in Section 2. The corresponding biological reactive behavior has been observed and studied in bees, and robotic analogs have been originally developed for nonholonomic mobile robots (see [31] and references therein). Adaptation to the significantly more complex dynamics of undulatory locomotors is discussed in Section 3 and highlights various issues related to the use of sensors for generating reactive behaviors for such systems. Such issues include, in particular, the modulation of the undulatory envelope, by adapting the amplitude of the body wave to the size of a specific corridor environment, based on information from sensors distributed over the elongated body of the mechanism. These issues are explored in simulation using the SIMUUN set of computational tools, which are specifically geared towards undulatory locomotion in robotics and biology [32]. Simulation results related to undulatory centering (implemented mostly via explicit joint angle control, but also via biomimetic neuromuscular control) are presented in Section 4. In this section, the use of centering for multi-undulatory swarms is also considered, complemented by sensor-based formation control in order to increase the cohesion of the swarm. A series of undulatory robotic prototypes has been developed, which are able to propel themselves on hard floor, on foam elastic material, on sand, on pebbles, etc., both in eel-like and in polychaete-like undulatory modes. These prototypes may use blade-like contact elements for propulsion on unstructured terrain, or wheeled modules for propulsion on hard surfaces. Our

undulatory prototypes have been equipped with infrared distance sensors, and their wheeled versions are used on hard planar surfaces to demonstrate the undulatory centering behavior in several corridor-like environments. Related experimental results are presented in Section 5.

## 2 Modelling Undulatory Locomotion

Undulatory locomotion is achieved through appropriate coupling of internal shape changes (typically a wave traveling along the body) to external motion constrains (typically frictional forces arising from the interaction with the locomotion environment). The main components involved in simulating an undulatory locomotor are: (i) the body mechanical model, (ii) the force model of the body's interaction with the environment and (iii) the body shape control strategy. The implementation of these components in the present study is described next.

### 2.1 Body Mechanics

The equations of motion of an undulatory robotic mechanism are obtained from its Lagrangian dynamics, after the reduction process described in [5, 33–36] and briefly outlined here. A computational model of a planar undulatory mechanism has been developed, based on a serial kinematic chain of $N$ rigid links (we consider $N$ odd; the case of $N = 7$ is shown in Figure 1). The links are considered to be identical and with the center of mass at the middle of each link. Each of the $N-1$ joint angles is considered to be independently actuated, to control the shape of the mechanism.

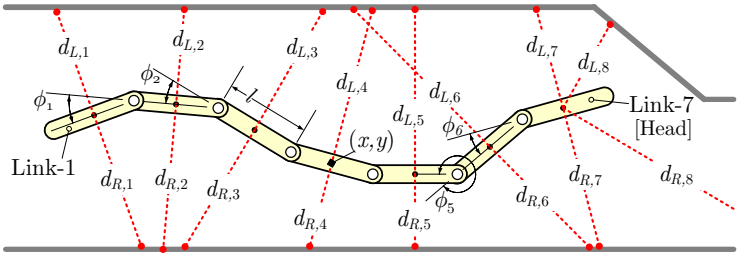


Figure 1. Computational model of a seven-link undulatory mechanism and its sensor array.

The position $(x, y)$ and orientation $\theta$ of the central link with respect to an inertial coordinate frame on the plane are the system's *group variables* and can be represented by an element $g$ of the group $G = SE(2)$, the Special Euclidean group of order 2. The Lie algebra element, corresponding to $g$, is $\xi \triangleq g^{-1}\dot{g} \in \mathcal{G} = se(2)$ and describes the *body velocity* of the central link. The joint angle vector $r = (\phi_1, \ldots, \phi_{N-1}) \in \mathcal{S} \triangleq S^{N-1}$denotes the *shape variables*, $\mathcal{S}$ the *shape space* of the system and $S$ the circle group. From the kinematics of the serial chain, it can be derived that the configuration of the mechanism is $q = (g, r) \in Q = G \times \mathcal{S} \triangleq SE(2) \times S^{N-1}$.

The Euler-Lagrange equations of motion can be reduced by exploiting the invariance of the mechanism to changes in inertial position and orientation, expressed as *Lie group symmetries* exhibited by the system. Assuming the existence of a Lagrangian function $L : TQ \to \mathbb{R}$ and of external forces $F : TQ \to T^*Q$ acting on the system, both of which are invariant under the action of the group $G$, a reduced Lagrangian $l$ can be determined, which is a function of $(r, \dot{r}, \xi)$ and takes the following form in body coordinates:

$$l(r, \dot{r}, \xi) = \frac{1}{2}\left(\xi^T \dot{r}^T\right) \begin{pmatrix} \mathbf{I}(r) & \mathbf{I}(r)\mathbf{A}(r) \\ \mathbf{A}^T(r)\mathbf{I}(r) & m(r) \end{pmatrix} \begin{pmatrix} \xi^T \\ \dot{r}^T \end{pmatrix} \tag{1}$$

The matrix $\mathbf{A}(r)$ is the local form of the *mechanical connection*, and depends only on the shape $r$. The *local locked inertia tensor* $\mathbf{I}(r)$ describes the total inertia of the system, when

all joints are frozen at a specific shape configuration $r$. The reduced equations of motion are, then, obtained in a body-fixed coordinate frame as:

$$\begin{aligned} \dot{g} &= g(-\mathbf{A}(r)\dot{r} + \mathbf{I}^{-1}(r)p), \\ \dot{p} &= ad^*_\xi p + f_T + f_N, \\ \tilde{M}(r)\ddot{r} + \dot{r}^T\tilde{C}(r)\dot{r} + \tilde{N} &= B(r)\tau, \end{aligned} \tag{2}$$

where $p$ is the body momentum, defined as $p \triangleq \partial l/\partial\xi$; the reduced matrices $\tilde{M}, \tilde{C}, \tilde{N}$ are detailed in [36]; $ad$ is the infinitesimal generator of the adjoint action of $G$ on $\mathcal{G}$; $f_T, f_N$ are the external frictional forces in the tangential and normal directions of the central link, related to $F$ as described in [36], and are obtained from the frictional force model employed as a function of the tangential and normal velocity of each link (see Section 2.2). The second equation above describes the evolution of momentum in body coordinates (not conserved in this coordinate frame) and is called the *momentum equation*. The third equation above is a second-order differential equation describing the evolution of the shape variables. Depending on the scheme used to generate the propulsive wave, the *controls* of the system can be either the joint torques $\tau$ (Section 2.3.2), or directly the joint angles $r$ (Section 2.3.1); this latter case is straightforward to implement, since the third equation in (2) can be decoupled from the rest of the system. The equations (2) are computationally efficient and well suited to controller development; they are also used to validate the equations of motion derived automatically by the Matlab® tools mentioned in Section 4.

## 2.2 Interaction with the Environment

In order to model the interaction of the undulatory mechanism with the environment (either terrestrial or aquatic), various resistive friction models have been utilized, in which the force on an individual body link comprises decoupled components in the normal and tangential direction of motion, both of which depend on the links' velocity (for details see [12, 32]). The sensor-based control schemes described in this study are able to generate various reactive behaviors in conjunction with any of these force models; for simplicity's sake, the simulations presented here utilize a viscous friction model, in which the tangential and normal components of the force applied to the $i$th link are obtained as:

$$F_T^i = -c_T v_T^i \quad \text{and} \quad F_N^i = -c_N v_N^i, \tag{3}$$

where $v_T^i$ and $v_N^i$ are the respective components of the velocity of the $i$th link.

The ratio $c_N/c_T$ of the force coefficients is a key parameter in undulatory locomotion. For $c_N > c_T$, the overall locomotion direction is *opposite* to that of the wave direction and, therefore, forward propulsion is achieved by a head-to-tail body wave. As exemplified by eels and snakes, this type of *eel-like* locomotion is by far the most common in nature, both on land and in the water, and it has been replicated in the vast majority of existing undulatory robots (e.g., [1–5,8,9,14,34]). For $c_N < c_T$, the locomotion is *along* the direction of wave propagation; hence forward motion is achieved by a tail-to-head wave. In nature, this locomotion mode is exhibited mainly by the polychaete annelid marine worms, but also by certain protozoa, flagellates and zoospores. Analysis of this novel type of *polychaete-like* undulatory locomotion and robotic prototypes implementing it, are described in [12].

## 2.3 Propulsive Wave Generation

The body shape control component is responsible for generating a traveling wave along the undulatory mechanism. The two methods employed to this purpose here, are described next.

### 2.3.1 Explicit joint angle control

The most straightforward way to explicitly generate a traveling wave in a serial chain of $N$ links (Figure 1) is by having the $N-1$ joint angles vary sinusoidally, with a common amplitude $A$, frequency $f$, angular offset $\psi$ and a constant phase lag $\phi_{lag}$ between consecutive joints. The time variation of the $i$th joint angle is:

$$\phi_i(t) = A\sin(2\pi ft + i\phi_{lag}) + \psi \tag{4}$$

This approach implies full control of the mechanism's joint angles, without consideration of the required torques. The propagation direction for the wave depends on the sign of the phase lag parameter, and is from link-$N$ to link-1 for $\phi_{lag} > 0$. The condition $\phi_{lag} = \pm 2\pi/N$ yields (exactly) one wavelength of the propulsive wave across the undulating body, with beneficial effects on the propulsive efficiency. The angular offset $\psi$ in eq. (4) provides a means for steering along curved paths, and is set to $\psi = 0$ for locomotion along a straight line. For $\psi \neq 0$, the resulting turning direction of the mechanism depends on the sign of $\psi$, as well as on the propagation direction of the wave (the sign of $\phi_{lag}$), and on the type of interaction with the environment (eel-like or polychaete-like).

Closed-loop control schemes utilizing eq. (4) may be set up, where the parameters $A$ and/or $f$ are used to modify the speed of locomotion, while changes in $\psi$ alter the heading direction [12].

For links of identical length, the formulation of eq. (4) produces a sinusoid-like body shape (shown in Figure 2 for a seven-link mechanism) which is an approximation of the *serpenoid curve* introduced in [1]; the equations provided therein can be used to obtain estimates of the body wave amplitude $B$ as a function of $A$ and $N$, which are used in closed-loop control (Appendix A).

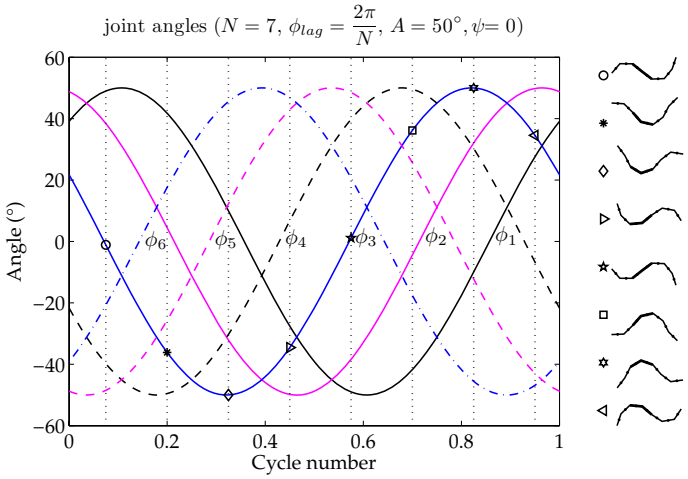


Figure 2. Relationship between the joint angles and the overall body shape for the explicit joint angle control scheme.

### 2.3.2 Neuromuscular control

Neuromuscular body shape control schemes have been developed [11, 17], based on models of the central pattern generator (CPG) which controls the undulatory swimming of the lamprey (e.g., [16,37,38]). These implement a connectionist CPG circuit, which is modelled as a chain of (identical) segmental oscillators, properly interconnected to generate a wave of joint activation. Each segmental oscillator comprises interneurons and motoneurons (all of which are modelled as leaky integrators), arranged in two symmetrical sub-networks that create oscillations through

mutual inhibition. The torque eventually applied to each of the body joints is determined by the outputs of the corresponding motoneurons, after they activate a pair of antagonistic lateral muscles, which are simulated using a spring-and-damper muscle model. The characteristics of the motoneuron outputs can be altered by tonic (i.e., non-oscillating) inputs to the left and right sub-networks of the segmental oscillators (denoted, respectively, by $I_L$ and $I_R$) [11, 17].

The locomotor CPG is coupled to the body mechanical model, and yields motion in a straight line for $I_L = I_R = I$, where the tonic input level $I$ alters the amplitude and frequency of the body wave via the motoneuron outputs. Turning motions of the mechanism are instigated by unequal tonic inputs to the two sides of the CPG. These tonic inputs are modulated by sensory information to implement the reactive behaviors described in Section 3. The successful generation of these behaviors depends on the intersegmental connectivity of the CPG, which affects critically the response of motoneurons to variations of the tonic input.

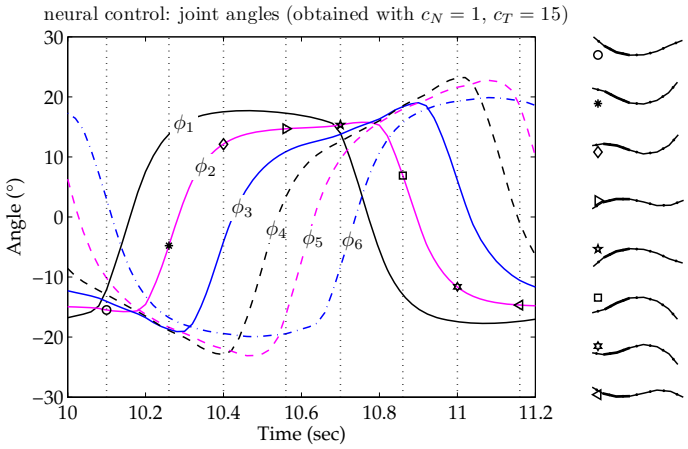


Figure 3. Joint angles and overall body shape, obtained with the CPG-based neuromuscular control scheme, for a seven-link undulatory mechanism.

Since the CPG-based approach provides torque signals to the joints, their exact angular motion depends on the mechanical properties of the segments, as well as on the parameters of the force model used for describing the interaction with the environment. Therefore, the resulting joint angles are, in general, different from the explicitly defined ones (cf. Figures 3 and 2).

Despite the considerably increased computational complexity of the CPG neural control scheme, a number of appealing characteristics (distributed architecture, potential robustness through redundancy, etc.) render it an interesting alternative for the motion control of undulatory robots.

## 3 Reactive Behaviors for Undulatory Robots

The elongated articulated body of undulatory robots changes continuously its shape as it moves in its environment, thus complicating the generation of sensor-based reactive behaviors. Systematic guidelines for the selection of the related parameters like the number, type and topology of sensors are currently lacking; however, the typical morphology of the corresponding biological organisms hints at a distributed sensing and control architecture [39–44]. We consider distance sensors placed on each robot link, which are employed to dynamically adjust the propulsive wave amplitude, while the head link may incorporate additional sensors (e.g., distance, vision), whose output is utilized in steering the mechanism.

Although the control schemes presented here assume infinite-range distance sensors, variations of these approaches, which consider proximity information provided by limited-range

sensors or by simple, whisker-like tactile switches, have also been successfully developed.

### 3.1 Reactive Centering Control

Bees exhibit a centering response when flying through narrow gaps, which has been attributed to their balancing the retinal motion perceived by each of their two wide field-of-view compound eyes. This has inspired the implementation of reactive centering schemes for nonholonomic mobile robots, where optical flow information from several distinct "looking" directions in the field of view of an on-board panoramic camera is employed directly in the control loop [31]. The mobile robot is assumed to be moving inside a "corridor" formed by obstacles, which can be locally approximated by two straight parallel walls. The task of implementing a centering response consists in using the angular velocity of the mobile robot to drive the lateral distance of the robot from the walls, as well as its orientation, to desired values corresponding to the middle of the corridor. A motion control scheme, asymptotically driving the scaled difference of inverse depths of the robot from the corridor walls to zero, can be shown to effectively address this task.

Adaptation of this sensor-based control scheme to the dynamics of undulatory robotic locomotors relies on balancing the weighted sum of the distance sensor outputs to the left and right sides of the robot. We consider $M$ pairs of distance sensors, distributed along the elongated body of the robot, and denote by $d_{L,j}$ and $d_{R,j}$ $(1 \leq j \leq M)$ the outputs for such a sensing array (Figure 1). The steering offset $\psi$ in eq. (4) is specified by the distance balancing metric $s(t)$, which is defined as:

$$s(t) = \frac{1}{\sum_{j=1}^{M} w_j d_{L,j}(t)} - \frac{1}{\sum_{j=1}^{M} w_j d_{R,j}(t)} \tag{5}$$

The weights $w_j$ in eq. (5) determine the relative contribution of each of the $M$ sensor pairs in calculating $s(t)$. For the explicit joint angle control scheme, the steering offset is set proportional to the distance balancing metric, i.e., $\psi(t) = k_e s(t)$, where $k_e$ is an appropriate gain. Therefore, the full joint angle control comprises a periodic component (first term below) and a sensor-based feedback component (second term), i.e.:

$$\phi_i(t) = A \sin(2\pi f t + i\phi_{lag}) + k_e s(t) \tag{6}$$

An averaging filter may be used to reduce the oscillatory variation of $s(t)$, due to the undulatory movement of the system:

$$\phi_i(t) = A \sin(2\pi f t + i\phi_{lag}) + \frac{k_e}{T} \int_{t-T}^{t} s(t)dt \tag{7}$$

This scheme applies a moving average filter, which spans the joint oscillation period $T = 1/f$, to the distance balancing metric, and yields a smoother control signal, at the expense of reduced responsiveness of the centering behavior.

For the neuromuscular control scheme, the distance balancing metric $s(t)$ is used to alter the tonic input signals applied to the left and right sides of the CPG, so that:

$$I_L(t) = I - k_n s(t) \quad \text{and} \quad I_R(t) = I + k_n s(t), \quad \text{for } k_n > 0 \tag{8}$$

In such schemes, the oscillation period of each joint depends in a complicated manner on tonic input. Therefore, implementing a moving average filter analogous to eq. (7) is an involved process.

### 3.2 Reactive Modulation of Undulatory Envelope

Reactive envelope modulation refers to the use of information from sensors distributed along the length of the undulatory mechanism to adjust the amplitude of the body wave, in order to allow the robot to navigate in environments involving variable corridor widths and/or tighter turns. Assuming ideal distance sensors, the approach adopted here involves an adaptive gain $k(t)$ multiplying all joint angle controls $\phi_i(t)$, which depends on the instantaneous value of the proximity ratio $B/d_{\min}$ ($d_{\min}$ is the minimum distance measured by the sensor array and $B$ is the body wave amplitude):

$$k(t) = k_1 + \frac{1}{T}\int_{t-T}^{t} \frac{k_2 - k_1}{1 + \exp\left(-c_1 \dfrac{B(t)}{d_{\min}(t)} + c_2\right)} dt \tag{9}$$

This implements an asymmetric sigmoidal gain of the proximity ratio ($k_1$ and $k_2$ are the lower and upper asymptotic values respectively, while the slope and the point of unit gain is specified via $c_1$ and $c_2$; see Figure 4), subsequently smoothed by a moving average filter which spans the joint oscillation period $T = 1/f$. The filtering stage improves robustness over abrupt changes in $d_{\min}$ (brought about e.g., by tight turns in complex structures) at the expense of some reduced responsiveness.

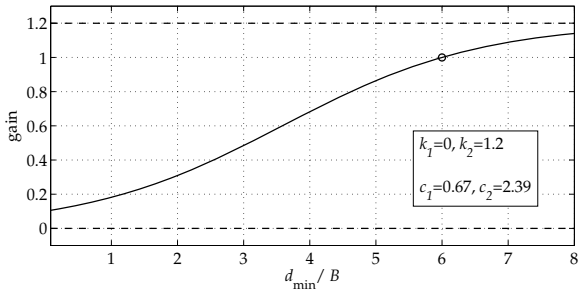


Figure 4. The asymmetric gain as a function of the inverse proximity ratio.

For the neural control scheme, modulation of the undulatory envelope can be obtained by applying a similar adaptive gain to both tonic input signals controlling the body CPG. Note however, that the required mapping of the tonic excitation level to the resulting body wave amplitude of the undulatory mechanism cannot be performed analytically and needs to be determined experimentally.

### 3.3 Formation Control of Undulatory Swarms

We consider now swarms of undulatory mechanisms in corridor-like environments. The previous reactive schemes can still be exploited by individual members of the swarm, in order to facilitate their traversal of such environments. However, if these reactive schemes are complemented by appropriate formation control components, increased coherence of the swarm may be obtained. Here we employ a variation of the "rectilinear" controller proposed in [27,28] for multiple unit-speed vehicles, where formations emerge by steering controls alone. Adaptation to a swarm of undulatory mechanisms, each under explicit joint angle control, involves setting the steering offset of the joint oscillations of the $j$th robot as:

$$\phi_{j,i}(t) = A_j \sin(2\pi f_j t + i\phi_{j,lag}) + \psi_j, \qquad j = 1...n$$

$$\psi_j = \frac{1}{n} \sum_{k \neq j} (-\eta \sin \varphi_j \cos \varphi_j + f(\rho_{jk}) \cos \varphi_j + \mu \sin(\varphi_k - \varphi_j)) \tag{10}$$

$$f(r) = a \left(1 - \left(\frac{r_0}{r}\right)^2\right)$$

where $\eta$, $\mu$, $a$ and $r_0$ are positive constants, while $n$ is the number of robots in the swarm. Considering the $(j,k)$-th pair of undulatory robots, $\rho_{jk}$ denotes the distance between the centers of their head links, while $\varphi_j$ and $\varphi_k$ denote the orientation of these head links with respect to the direction perpendicular to the baseline connecting the centers of the head links (Figure 5). Such sensory information might be obtained e.g., by a combination of panoramic cameras (for determining the relative orientation) and scanning laser sensors (for obtaining range estimates). Finally, these formation control schemes can also be adapted for use with the CPG-based neural controllers [17].

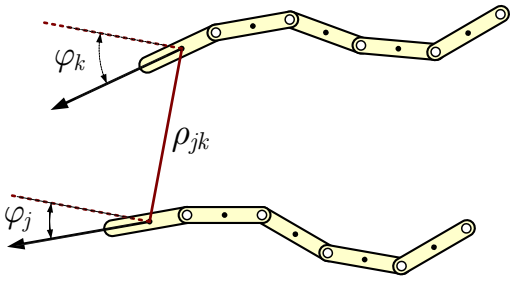


Figure 5. Definition of the distance and orientation terms in eq. (10), for a pair of undulatory robots.

## 4 Simulation Results

The simulation studies implementing the reactive behaviors proposed above are based on an undulatory mechanism composed of $N = 7$ identical links, each equipped with a distance sensor pair aiming at $\pm 90^\circ$ with respect to the link's main axis, while the head link features an additional pair of distance sensors, aiming at $\pm 45^\circ$ (Figure 1). Simulations are set up using the SIMUUN simulation environment, which provides computational models for mechanical, control, neural control and sensory aspects of undulatory locomotion within a Matlab/Simulink framework [32]. SIMUUN includes modules which emulate distance sensing elements, as well as implement simple 2D models of the world that the mechanism operates in. These are used to set up the sensor array for the seven-link mechanism, and to construct corridor-like environments of varying complexity to test the performance of the centering controller, both for explicit joint angle control and for CPG-based schemes of generating the traveling wave.

### 4.1 Undulatory Centering with Explicit Joint Angle Control

The efficacy of the undulatory centering controller utilizing (5)-(6) was investigated in a series of simulations, carried out over a range of $c_N/c_T$ values, that involved both eel-like and polychaete-like interaction with the environment. The body wave parameters were set as $A = 28^\circ$, $\phi_{lag} = 2\pi/N$, and simulations were performed for different values of the controller gain in eq. (6), initially considering the geometry of parallel-sided corridors with a width equal to $L$ or $2L$,

where $L$ is the total length of the mechanism. Subsequent trajectory plots are normalized with respect to the body length $L$.

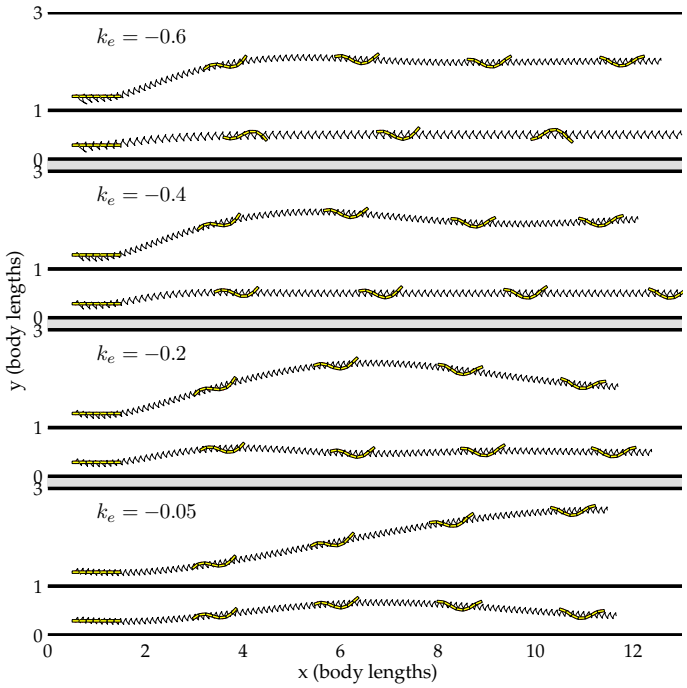


Figure 6. Centering behavior utilising sensor data from the head link, for polychaete-like interaction with the environment ($c_N/c_T = 0.025$).

The centering behavior was successfully implemented for both eel-like and polychaete-like undulatory locomotion, utilizing data only from the head sensors. The speed of convergence along the center of the corridor was found to depend both on the gain $k_e$ and on the corridor width (as illustrated in Figure 6 for polychaete-like locomotion), while the $c_N/c_T$ ratio had little impact on the trajectory followed. However, further study of the impact of the spatio-temporal sensory data characteristics on controller response, appears to be required, especially for polychaete-like locomotion.

The control scheme's ability to generate the centering behavior on corridor areas comprising different types of substrates is demonstrated in Figure 7. The somewhat reduced responsiveness of the filtered variation of the centering controller in eq. (7), is demonstrated in Figure 8.

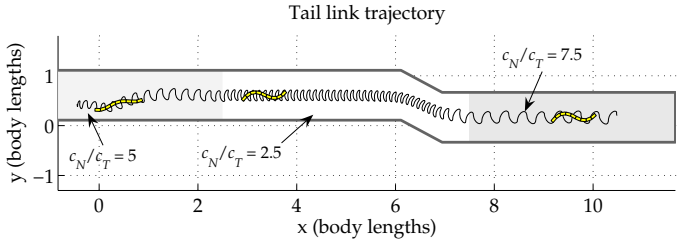


Figure 7. Undulatory centering behavior over a locomotion environment with different characteristics (shown for eel-like interaction with the environment).

Incorporating the sensor-based envelope modulation scheme in the previously-described centering controller allows navigation of the complex corridor-like structure in Figure 9 without the mechanism coming into contact with the corridor walls; this is not the case when using

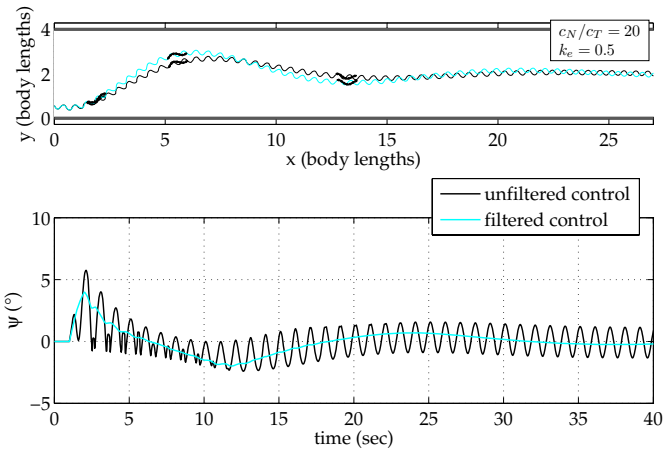


Figure 8. Trajectory and control signals for the filtered version of the centering control law.

the centering controller alone. Additionally, it is possible to increase the undulation amplitude (and therefore the locomotion speed) when traversing wider corridor sections.

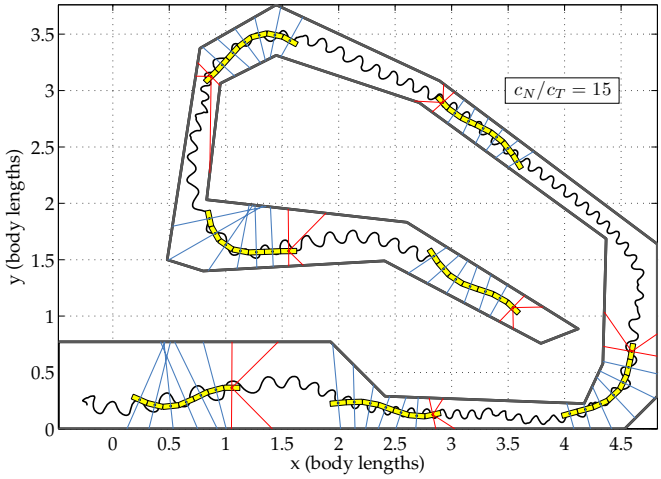


(a) - tail link trajectory

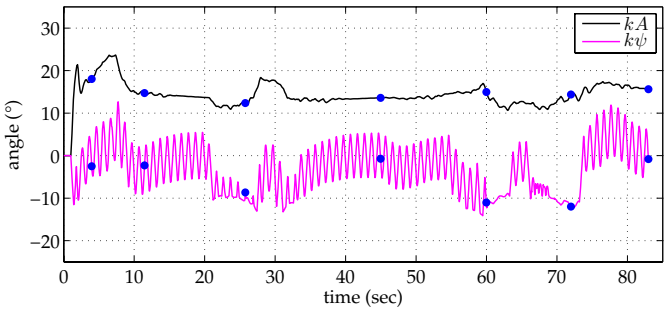


(b) - body wave controls

Figure 9. Combining reactive centering and envelope modulation to navigate a complex corridor. The nominal joint oscillation amplitude is $A = 30°$. In the trajectory plot, blue lines denote the sensed distances which are used for envelope modulation alone; the markers in (b) correspond to the mechanism snapshots shown in (a).

### 4.2 Undulatory Centering with Neural Control

The reactive centering behavior may be implemented in a more biomimetic way using neuromuscular control schemes via an appropriate CPG neural circuit. The CPG developed here comprises 20 segmental oscillators, with the motoneuron outputs from (roughly) every third oscillator utilized to provide torque signals to the six joints of the seven-link mechanism, through the activation of antagonistic muscles. A series of simulations demonstrates the ability of the integrated neural control scheme to successfully navigate the robot through various corridor-like courses, both for eel-like and for polychaete-like interaction with the environment, when utilizing sensory information from the head link. Indicative results are shown in Figure 10 [11,17].

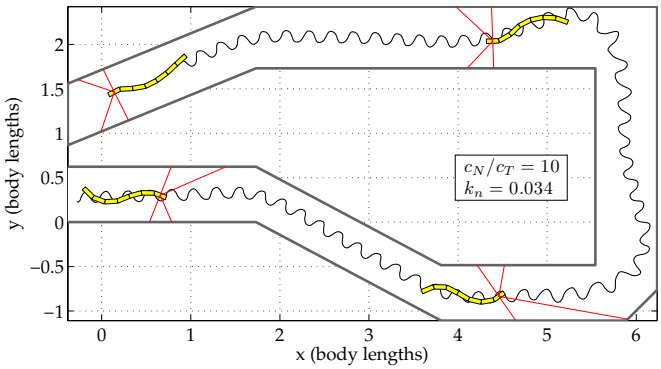


(a) - tail link trajectory

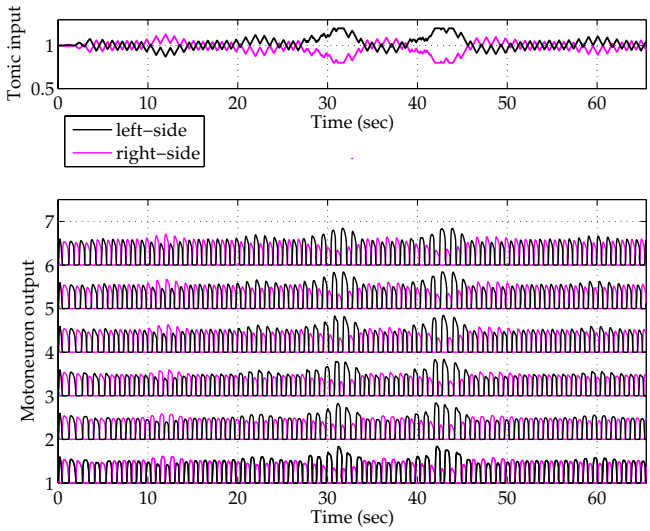


(b) - neural control

Figure 10. Neural control of the undulatory centering behavior, for eel-like locomotion: (a) trajectory of the mechanism, and (b) the corresponding tonic input signals and motoneuron outputs of the locomotor CPG.

### 4.3 Formation Control of Undulatory Swarms

Simulations of multiple undulatory mechanisms, each one implementing the reactive centering behavior, were carried out, demonstrating that this scheme is well suited to the traversal of corridor-like environments by a swarm. In particular, when the swarm configuration involved two or more mechanisms moving side-to-side, a distribution of them along the corridor width emerged as a consequence of each one essentially forming a moving boundary for the centering behavior of the adjacent mechanisms. Integrating reactive envelope modulation with the centering control, in each undulatory mechanism, affords improved collision avoidance and greater

versatility with regard to the complexity of the course to be traversed.

Increased swarm coherence may be obtained by implementing appropriate formation control laws, as described in Section 3.3. The standalone rectilinear formation control law of eq. (10) is demonstrated, in a follow-the-leader context, for a swarm of $n = 4$ undulatory robots in Figure 11. Indicative results from simulations involving undulatory robots under both formation and centering control, are shown in Figure 12.

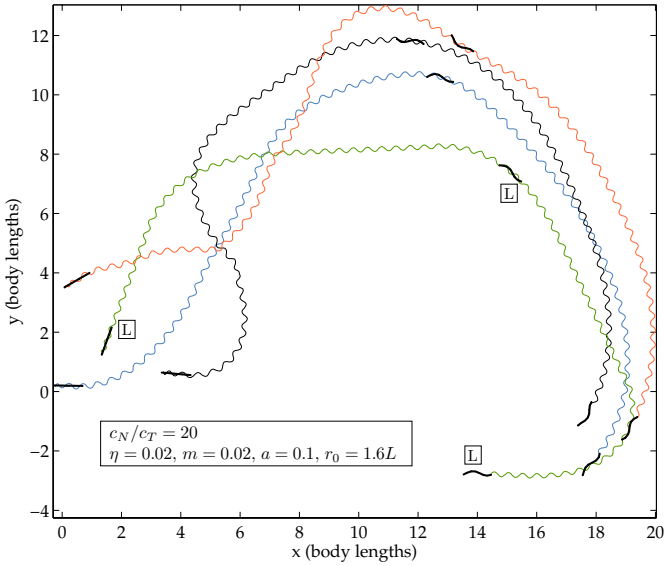


Figure 11. The rectilinear control law, implemented for a swarm of $n = 4$ undulatory robots. The robot labeled with $L$ is the leader, whose movements are tracked by the other swarm members, which also maintains a tight formation, as the swarm moves from left to right.

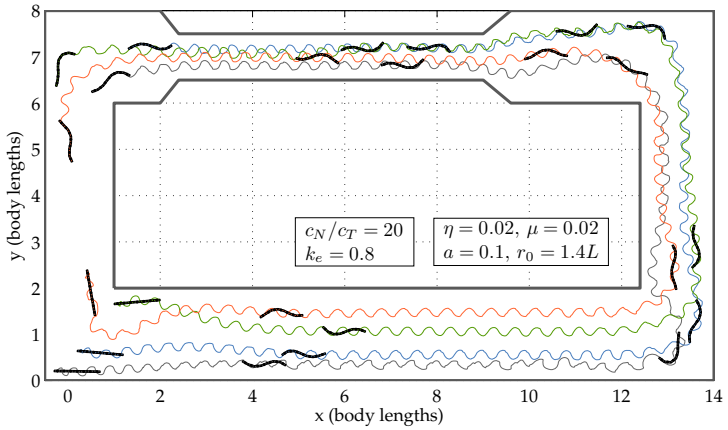


Figure 12. Swarm of $n = 4$ undulatory robots maintains its cohesion while traversing a corridor environment. The initial swarm configuration is shown on the lower left corner of the figure.

## 5 Experiments

In order to experimentally evaluate the reactive behaviors presented in the previous sections, a series of undulatory robotic prototypes has been developed, using off-the-shelf components and conventional fabrication techniques (see also [12]). The prototype used in the present study, shown in Figure 13a, is composed of 5 aluminium links (weight 130 g, length 95 mm,

width 50 mm), with the rotary joints actuated by high-torque R/C servo-motors (*HiTech* HSR-5995TG). The underside of the links has been appropriately designed to allow the attachment of different modules, which implement the interaction with the locomotion environment by providing differential friction in the tangential and normal directions of motion. For movement over relatively smooth surfaces, wheeled modules are used (Figure 13b), which may be mounted either longitudinally or transversally with respect to the link's axis, in order to yield eel-like or polychaete-like locomotion, respectively. For movement over unstructured environments, such as sand, pebbles and mud, special modules, shown in Figure 13c, have also been developed, which employ aluminium blades (whose number and spacing can be easily changed).

An on-board microcontroller unit (*Motorola* DSP56807) is used to generate the propulsive wave and to implement the controllers for the reactive behaviors, using input from infrared distance sensors (*Sharp* GP2Y0A02YK and GP2D12 units have been used). Data from the prototype during the experiments are wirelessly transmitted to a PC ground station via a bluetooth-based serial link. This hardware setup allows for fully autonomous operation of the undulatory mechanism, when it is powered by the on-board batteries; alternatively, an external power supply can be used during extended testing sessions.

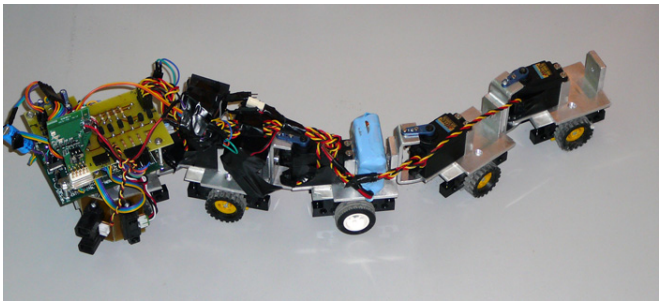

(a)

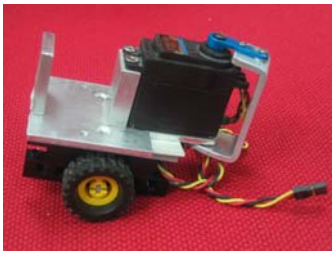

(b) wheeled module

(c) blade module

Figure 13. (a) The five-link undulatory robotic prototype. (b)-(c) Two different contact modules, mounted longitudinally on a link of the robot.

In order to trace the movements performed by the tail link of the mechanism during experiments, an orange-coloured marker ball has been mounted on it. Post-processing of the experiment videos with standard image processing procedures can then provide a steady tracking of the marker's position throughout the video frames, thus allowing the accurate reconstruction of the tail link trajectory.

In the experiments presented here, reactive centering was demonstrated for the eel-like undulatory locomotion mode on hard floor, using the wheeled modules mounted longitudinally under the links. The centering behavior has been implemented via the explicit joint angle control scheme, as described by eqs. (6)-(7), using a joint angle amplitude of $A = 45°$, a phase lag of $\phi_{lag} = 2\pi/N$, and a joint oscillation frequency of $f = 1\,\text{Hz}$, while the controller gain is set to $k_e = 0.3$. The distance balancing metric of eq. (5) is calculated using the output from two pairs of infrared distance sensors, which are mounted on the head link and aim at $\pm 45°$and $\pm 90°$ (i.e., replicating the sensor array configuration used in the simulations of Sections 4.1-4.2),

with the respective weights set to $w_1 = w_2 = 1$.

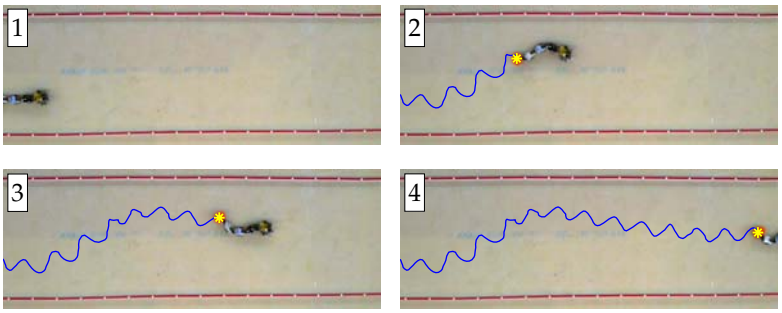


Figure 14. Snapshots of the trajectory of the undulatory robot, implementing the reactive centering behavior while moving over a plywood board in a straight corridor.

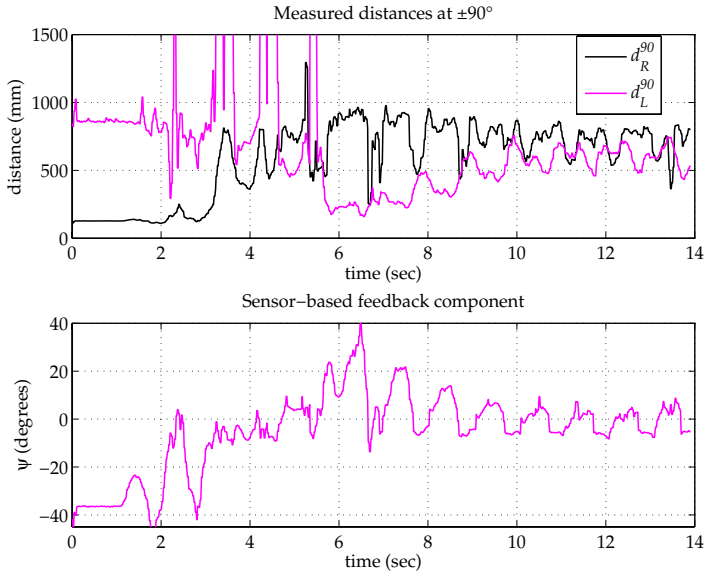


Figure 15. Data from the experiment of Figure 14: Data from the infrared distance sensors (top) and sensor-based feedback component $\psi$ of the joint angle controls (bottom).

Experiments were performed on a variety of hard surfaces (e.g., wood, tiling, marble) and for different corridor layouts, which were constructed using a set of modular brick-like elements. Initial experiments involving straight-line corridor segments confirmed the efficacy of the proposed scheme, using both the unfiltered and filtered variants for the sensor-based feedback component $\psi$. Although the unfiltered controls of eq. (6) yielded increased responsiveness, the filtered ones in eq. (7) provided smoother robot trajectories, as well as robustness against noise in the sensor measurements. Results from one such experiment, involving a 1 m-wide corridor laid out on a plywood board, and using the unfiltered variant of the centering controller, are provided in Figures 14 and 15. The reconstructed trajectory (Figure 14) indicates that, following an initial overshoot, the robot manages to successfully settle to and maintain a route which is, on the average, along the corridor center. The data sent by the robot during the course of this experiment are shown in Figure 15. More specifically, the distances measured by the sensor pair aiming at $\pm 90^\circ$ can be seen to start at different levels, corresponding to the initial configuration of the mechanism (see Figure 14), and progressively converge to the same, on the average, mean value. The oscillatory character of these signals is directly related to the undulatory movement of the robot, while the imperfect nature of the sensing elements is

manifested in the noise present in the measurements, as well as in the spurious values observed (e.g., between $t = 2\,\mathrm{s}$ and $t = 6\,\mathrm{s}$) These sensory data are used to calculate the sensor-based feedback component $\psi$ of the joint angle controls, which can be seen to settle to a mean value of zero, and whose oscillatory nature highlights the use of the unfiltered variant of the centering controller.

Having successfully implemented the centering behavior for straight corridors, a set of experiments was then carried out involving more complex courses. Using the same body wave and control parameters as before, the robot successfully navigated these routes, as it is demonstrated by the trajectory snapshots shown in Figure 16. These were obtained using the filtered variant of the centering controller.

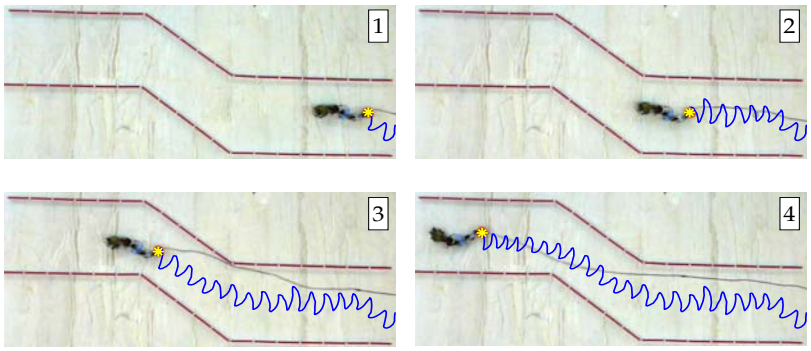


(a)

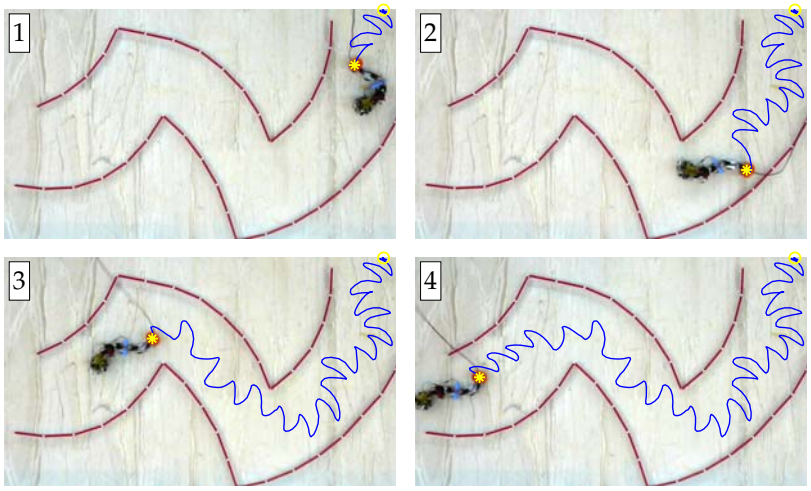


(b)

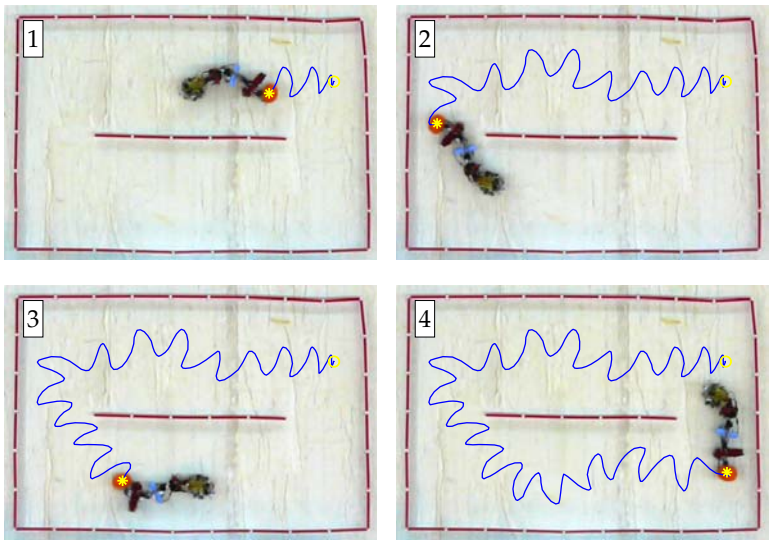


(c)

Figure 16. Snapshots of the trajectory of the undulatory robot implementing the reactive centering behavior, while moving over hard floor along different corridor routes.

# 6 Conclusions

Several closed-loop control schemes, giving rise to reactive behaviors for undulatory robots, have been presented, and evaluated in simulation, as well as experimentally. A biomimetic centering behavior has been implemented, both by explicit body shape control and by neuromuscular control of body undulations. Formation control for swarms of multiple undulatory robots has been demonstrated in narrow corridor-like environments, which in conjunction with centering control, allows the swarm robots to maintain the cohesion of their group while navigating in these environments. Experiments with an undulatory robotic prototype have validated the proposed control scheme for reactive centering, demonstrating the successful navigation of various corridor-like environments, while exhibiting a robust performance with respect to sensor noise.

Future work will concentrate on alternative sensory modalities (e.g., vision), as well as on the in-depth analysis and implementation of the sensors' distribution along the body of the undulatory mechanism, considering the effects of the body undulations on the feedback and control signals of the system. Further experiments with the robotic prototype will evaluate the performance of these reactive schemes in a greater variety of locomotion environments, focusing on unstructured substrates (e.g., sand, pebbles and mud) for which the robot has already successfully demonstrated open-loop gait generation (cf. [12]). Finally, a distributed architecture for the robot controller is currently under investigation, allowing the implementation of more complex schemes, including CPG-based neural control.

# Acknowledgment

Related papers and videos of the experimental results presented here can be found at the Web site *www.ics.forth.gr/~tsakiris*.

# References

[1] S. Hirose, *Biologically Inspired Robots: Snake-Like Locomotors and Manipulators*. New York: Oxford University Press, 1993.

[2] S. Hirose and E. Fukushima, "Snakes and strings: New robotic components for rescue operations," *International Journal of Robotics Research*, vol. 23, no. 4/5, pp. 341–349, 2004.

[3] J. Ostrowski and J. Burdick, "The geometric mechanics of undulatory robotic locomotion," *International Journal of Robotics Research*, vol. 17, no. 7, pp. 683–701, 1998.

[4] S. Ma, "Development of a creeping locomotion snake-robot," *International Journal of Robotics and Automation*, vol. 17, no. 4, pp. 146–153, 2002.

[5] P. Krishnaprasad and D. Tsakiris, "Oscillations, SE(2)-snakes and motion control: A study of the roller racer," *Dynamical Systems*, vol. 16, no. 4, pp. 347–397, 2001.

[6] M. Yamakita, M. Hashimoto, and T. Yamada, "Control of locomotion and head configuration of 3d snake robot (SMA)," in *Proc. IEEE Int. Conf. on Robotics and Automation (ICRA'03)*, Taipei, Taiwan, 2003, pp. 2055–2060.

[7] R. Worst and R. Linnemann, "Construction and operation of a snake-like robot," in *Proc. IEEE Int. Joint Symp. on Intelligence and Systems*, 1996, pp. 164–169.

[8] M. Saito, M. Fukaya, and T. Iwasaki, "Modeling, analysis, and synthesis of serpentine locomotion with a multilink robotic snake," *IEEE Control Systems Magazine*, vol. 22, no. 1, pp. 64–81, 2002.

[9] L. Chen, S. Wang, S. Ma, and B. Li, "Analysis of traveling wave locomotion of snake robot," in *Proc. IEEE Int. Conf. on Robotics, Intelligent Systems and Signal Processing (RISSP'03)*, Changsha, China, 2003, pp. 365–369.

[10] H. Choset *et al.*, *Modular Serpentine Robot Locomotion*, Sensor Based Planning Lab, Carnegie Mellon University, *http://www.modsnakes.com*.

[11] D. Tsakiris, A. Menciassi, M. Sfakiotakis, G. La Spina, and P. Dario, "Undulatory locomotion of polychaete annelids: mechanics, neural control and robotic prototypes," in *Abstracts book of The Annual Computational Neuroscience Meeting (CNS*2004)*, Abstract #288, Poster #M69, Baltimore, USA, 2004, p. 89.

[12] D. Tsakiris, M. Sfakiotakis, A. Menciassi, G. La Spina, and P. Dario, "Polychaete-like undulatory robotic locomotion," in *Proc. IEEE Int. Conf. on Robotics and Automation (ICRA'05)*, Barcelona, Spain, 2005, pp. 3029–3034.

[13] J. Ayers, C. Wilbur, and C. Olcott, "Lamprey robots," in *Proc. Int. Symp. on Aqua Biomechanisms*, T. Wu and N. Kato, Eds., 2000.

[14] J. Ayers, *Neurotechnology for Biomimetic Robots*, J. L. Davis and A. Rudolph, Eds. Cambridge: MIT Press, 2003.

[15] K. McIsaac and J. Ostrowski, "Experiments in closed-loop control for an underwater eel-like robot," in *Proc. IEEE Int. Conf. on Robotics and Automation (ICRA'02)*, Washington, DC, USA, 2002, pp. 750–755.

[16] A. Crespi, A. Badertscher, A. Guignard, and A. Ijspeert, "Amphibot I: an amphibious snake-like robot," *Robotics and Autonomous Systems*, vol. 50, no. 4, pp. 163–175, 2005.

[17] M. Sfakiotakis and D. Tsakiris, "Neuromuscular control of reactive behaviors for undulatory robots," *Neurocomputing*, Elsevier B.V., (conditionally accepted for publication).

[18] P. Prautsch and T. Mita, "Control and analysis of the gait of snake robots," in *Proc. IEEE Int. Conf. on Control Applications (CCA'99)*, 1999, pp. 502–507.

[19] S. Ma, Y. Ohmameuda, K. Inoue, and B. Li, "Control of a 3-dimensional snake-like robot," in *Proc. IEEE Int. Conf. on Robotics and Automation (ICRA'03)*, Taipei, Taiwan, 2003, pp. 2067–2072.

[20] B. Li, S. Ma, Y. Wang, Y. lv, and L. Chen, "Environment-adaptable locomotion of a snake-like robot," in *Proc. IEEE Int. Conf. on Robotics and Biomimetics (ROBIO'04)*, Shenyang, China, 2004, pp. 584–588.

[21] B. Klaassen and K. Paap, "GMD-SNAKE2: A snake-like robot driven by wheels and a method for motion control," in *Proc. IEEE Int. Conf. on Robotics and Automation (ICRA'96)*, 1999, pp. 3014–3019.

[22] M. Kolesnik and H. Streich, "Visual orientation and motion control of MAKRO - adaptation to the sewer environment," in *Proc. 7th Int. Conf. on Simulation of Adaptive Behavior*, 2002, pp. 62–69.

[23] L. Xinyu and F. Matsuno, "Control of snake-like robot based on kinematic model with image sensor," in *Proc. IEEE Int. Conf. on Robotics, Intelligent Systems and Signal Processing (RISSP'03)*, Changsha, China, 2003, pp. 347–352.

[24] C. Ye, S. Ma, B. Li, and Y. Wang, "Turning and side motion of a snake-like robot," in *Proc. IEEE Int. Conf. on Robotics and Automation (ICRA'04)*, New Orleans, USA, 2004, pp. 5075–5080.

[25] A. Jadbabaie, J. Lin, and A. Morse, "Coordination of groups of mobile autonomous agents using nearest neighbor rules," *IEEE Transactions on Automatic Control*, vol. 48, no. 6, pp. 988–1001, 2003.

[26] P. Ögren and N. Leonard, "Obstacle avoidance in formation," in *Proc. IEEE Int. Conf. on Robotics and Automation (ICRA'03)*, Taipei, Taiwan, 2003, pp. 2492–2497.

[27] E. Justh and P. Krishnaprasad, "A simple control law for UAV formation flying," Technical Report TR-2002-38, Institute for Systems Research, University of Maryland, College Park, 2002.

[28] ——, "Equilibria and steering laws for planar formation," *Systems and Control Letters*, vol. 52, no. 1, pp. 25–38, 2004.

[29] R. Vidal, O. Shakernia, and S. Sastry, "Following the flock," *IEEE Robotics and Automation Magazine*, vol. 11, no. 4, pp. 14–20, 2004.

[30] M. Dorigo, et al, "Evolving self-organizing behaviors for a Swarm-bot," *Autonomous Robots*, vol. 17, no. 2/3, pp. 223–245, 2004.

[31] A. Argyros, D. Tsakiris, and C. Groyer, "Biomimetic centering behavior for mobile robots with panoramic sensors," *IEEE Robotics and Automation Magazine*, vol. 11, no. 4, pp. 21–30, 2004.

[32] M. Sfakiotakis and D. Tsakiris, "SIMUUN: A simulation environment for undulatory locomotion," *International Journal of Modelling and Simulation*, IASTED/Acta Press, in press.

[33] A. Bloch, P. Krishnaprasad, J. Marsden, and R. Murray, "Nonholonomic mechanical systems with symmetry," *Archive for Rational Mechanics and Analysis*, vol. 136, pp. 21–99, 1996.

[34] J. Cortes, S. Martinez, J. Ostrowski, and K. McIsaac, "Optimal gaits for dynamic robotic locomotion," *International Journal of Robotics Research*, vol. 20, no. 9, pp. 707–728, 2001.

[35] J. Marsden and T. Ratiu, *Introduction to Mechanics and Symmetry.* Springer-Verlag, 1994.

[36] R. Murray, "Nonlinear control of mechanical systems: a Lagrangian perspective," *Annual Reviews in Control*, vol. 21, pp. 31–42, 1997.

[37] Ö. Ekeberg and S. Grillner, "Simulations of neuromuscular control in lamprey swimming," *Philosophical Transactions of the Royal Society of London Series B*, vol. 354, no. 1385, pp. 895–902, 1999.

[38] A. Ijspeert, "A connectionist central pattern generator for the aquatic and terrestrial gaits of a simulated salamander," *Biological Cybernetics*, vol. 85, no. 5, pp. 331–348, 2001.

[39] J. Gray, "Annelids," in *Animal Locomotion.* London: Weidenfeld & Nicolson, 1968, pp. 377–410.

[40] R. Brusca and G. Brusca, *Invertebrates.* Sunderland: Sinauer Associates, 1990.

[41] J. Lawry, "Mechanisms of locomotion in the polychaete *Harmothoë*," *Comparative Biochemistry and Physiology*, vol. 37, no. 2, pp. 167–179, 1970.

[42] F. Eisenhart, T. Cacciatore, and W. Kristian Jr., "A central pattern generator underlies crawling in the medicinal leech," *Journal of Comparative Physiology A*, vol. 186, pp. 631–643, 2000.

[43] G. Orlovsky, T. Deliagina, and S. Grillner, *Neuronal Control of Locomotion: from Mollusc to Man.* Oxford: Oxford University Press, 1999.

[44] E. Niebur and P. Erdös, "Modeling locomotion and its neural control in nematodes," *Comments on Theoretical Biology*, vol. 3, no. 2, pp. 109–139, 1993.

[45] M. Abramowitz and I. A. Stegun, *Handbook of Mathematical Functions with Formulas, Graphs, and Mathematical Tables*, ninth dover printing, tenth gpo printing ed. New York: Dover, 1964.

## Appendix A: Amplitude of the Body Wave

For links of identical length $l$, the relative angles between successive links $\phi_i$ described in eq. (4), relate to an overall body shape for the mechanism which is an approximation of a *serpenoid curve.* The serpenoid family of curves [1] describes the natural shape adopted by snakes during undulatory movements. Points along these curves are defined as

$$x(s) = \int_0^s \cos(\xi)d\sigma \quad , \quad y(s) = \int_0^s \sin(\xi)d\sigma \quad \text{where} \quad \xi = a\cos(b\sigma) + c\sigma \tag{11}$$

and where $s$ denotes arc length. The serpenoid curve has a periodic shape resembling a sinusoid, which is shaped by the parameters $a$ (degree of undulation), $b$ (number of periods per unit length) and $c$ (overall curvature). The relationship between the parameters of eqs. (4) and (11) are [8]

$$a = \frac{A}{2\left|\sin(\frac{\phi_{lag}}{2})\right|} \quad , \quad b = N\phi_{lag} \quad \text{and} \quad c = \psi N \tag{12}$$

These expressions can be used to obtain estimates of the body wave amplitude $B$ as a function of $A$ and $N$, when $\phi_{lag} = 2\pi/N$:

$$B(A, N) = L\int_0^{1/4} \sin\left(\frac{A}{2\left|\sin(\pi/N)\right|}\cos(2\pi\sigma)\right)d\sigma \tag{13}$$

where $L = Nl$ is the total length of the mechanism (Figure 17). Eq. (13) can be written as

$$B(a) = L\frac{\pi}{2}H_0(a) \tag{14}$$

where $H_0(x)$ is the Struve function [45]. In order to improve the computational efficiency of the online calculation of $B$ (e.g., for implementing closed-loop reactive behaviors, such as the one presented in Section 3.2), eq. (14) can be approximated by the first four terms of the respective power series expansion of $H_0(z)$ [45]:

$$B(a) = L\left(a - \frac{1}{9}a^3 + \frac{1}{225}a^5 - \frac{1}{11025}a^7\right) \tag{15}$$

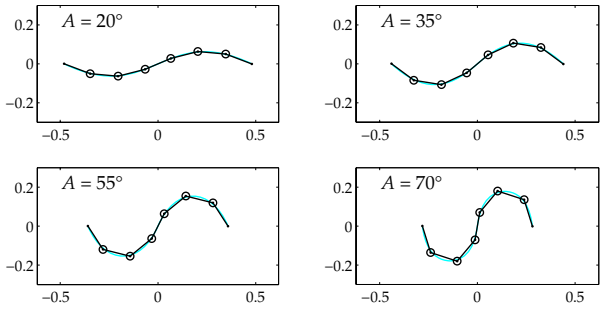


(a)

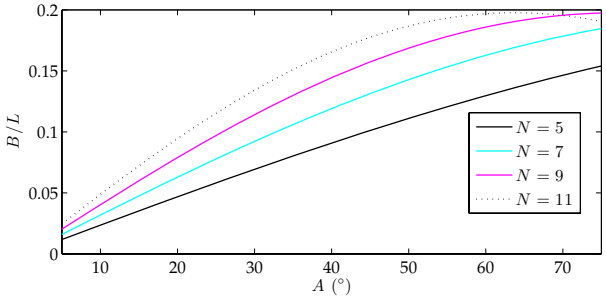


(b)

Figure 17. (a) Approximation of the body shape with the equivalent serpenoid curve for $\phi_{lag} = 2\pi/N$ and $\psi = 0$, for different values of the joint angle amplitude $A$. (b) The body wave amplitude $B$ (normalized by the body length $L$) as a function of $A$ and N.